TISSUE ENGINEERING: Part A
Volume 26, Numbers 15 and 16, 2020

DOI: 10.1089/ten.tea.2019.0222

termis
Tissue Engineering
& Regenerative Medicine
International Society

ORIGINAL ARTICLE

Acellular Biologic Nipple–Areolar Complex Graft: *In Vivo* Murine and Nonhuman Primate Host Response Evaluation

Nicholas C. Pashos, PhD,[1–4] David M. Graham, PhD,[3] Brian J. Burkett, MD,[5] Ben O'Donnell, BS,[1,2] Rachel A. Sabol, MS,[1,6] Joshua Helm, MS,[1,6] Elizabeth C. Martin, PhD,[7] Annie C. Bowles, PhD,[1] William M. Heim, MS, CTBS,[3] Vince C. Caronna, BS,[3] Kristin S. Miller, PhD,[8] Brooke Grasperge, DVM,[4] Scott Sullivan, MD, FACS,[9] Abigail E. Chaffin, MD, FACS,[10] and Bruce A. Bunnell, PhD[1,4,6]

There are more than 3 million breast cancer survivors living in the United States of which a significant number have undergone mastectomy followed by breast and nipple–areolar complex (NAC) reconstruction. Current strategies for NAC reconstruction are dependent on nonliving or nonpermanent techniques, including tattooing, nipple prosthetics, or surgical nipple-like structures. Described herein is a tissue engineering approach demonstrating the feasibility of an allogeneic acellular graft for nipple reconstruction. Nonhuman primate (NHP)-derived NAC tissues were decellularized and their extracellular matrix components analyzed by both proteomic and histological analyses. Decellularized NHP nipple tissue showed the removal of intact cells and greatly diminished profiles for intracellular proteins, as compared with intact NHP nipple tissue. We further evaluated the biocompatibility of decellularized grafts and their potential to support host-mediated neovascularization against commercially available acellular dermal grafts by performing *in vivo* studies in a murine model. A follow-up NHP pilot study evaluated the host-mediated neovascularization and re-epithelialization of onlay engrafted decellularized NAC grafts. The murine model revealed greater neovascularization in the decellularized NAC than in the commercially available control grafts, with no observed biocompatibility issues. The *in vivo* NHP model confirmed that the decellularized NAC grafts encourage neovascularization as well as re-epithelialization. These results support the concept that a biologically derived acellular nipple graft is a feasible approach for nipple reconstruction, supporting neovascularization in the absence of adverse systemic responses.

Keywords: breast cancer, breast reconstruction, nipple reconstruction, acellular biological matrix, nipple-areolar complex

Impact Statement

Currently, women in the United States most often undergo a mastectomy, followed by reconstruction, after being diagnosed with breast cancer. These breast cancer survivors are often left with nipple–areolar complex (NAC) reconstructions that are subsatisfactory, nonliving, and/or nonpermanent. Utilizing an acellular biologically derived whole NAC graft would allow these patients a living and permanent tissue engineering solution to nipple reconstruction.

[1]Center for Stem Cell Research and Regenerative Medicine, Tulane University School of Medicine, New Orleans, Louisiana, USA.
[2]Bioinnovation PhD Program, Tulane University, School of Science and Engineering, New Orleans, Louisiana, USA.
[3]BioAesthetics Corporation, Research Triangle Park, North Carolina, USA.
[4]Tulane National Primate Research Center, Covington, Louisiana, USA.
[5]Department of Radiology, Mayo Clinic, Rochester, Minnesota, USA.
[6]Department of Pharmacology, Tulane University School of Medicine, New Orleans, Louisiana, USA.
[7]Department of Biological and Agricultural Engineering, Louisiana State University, Baton Rouge, Louisiana, USA.
[8]Department of Biomedical Engineering, Tulane University, School of Science and Engineering, New Orleans, Louisiana, USA.
[9]Center for Restorative Breast Surgery, New Orleans, Louisiana, USA.
[10]Department of Surgery, Tulane University School of Medicine, New Orleans, Louisiana, USA.

Introduction

More than 268,000 new cases of female breast cancer are expected in the United States in 2019, and an estimated 2470 cases of breast cancer were diagnosed in men in 2017.[1,2] While incidence rates have remained relatively stable with a 0.2% annual increase for 2005–2014, mortality rates have declined annually by 1.8% for the same period.[3] This decline in mortality can be attributed to improvements in both early detection and treatment, with mastectomies representing a growing trend in treatment options.[2] The Agency for Healthcare Research and Quality (AHRQ) found that there was a 21% increase, from 74 per 100,000 women to 90 per 100,000 women, in the overall rate of mastectomies (combining single and double) from 2005 to 2013.[4]

Although reconstructive surgeons have practically perfected breast mound reconstruction, and if nipple-sparing mastectomy is not an option, nipple–areolar complex (NAC) reconstruction remains a challenge and the limiting factor for a complete breast reconstruction.[5–10] Importantly, NAC reconstruction is associated with improved psychosocial well-being and is critical to giving the breast reconstruction patient a sense of completeness and closure to her cancer experience.[8,11–16] Studies have shown that the NAC may play as significant of a role in psychological well-being as the reconstructed breast mound.[13,17,18] Patients continue to feel distress after breast mound reconstruction, up until NAC reconstruction.[17] NAC reconstruction is highly correlated with self-esteem and improved body image, and women with NAC reconstruction have significantly higher sexual well-being, aesthetic and general satisfaction, and quality-of-life scores, as compared with women without NAC reconstruction.[8,13,14,16–19]

Despite the widespread popularity and health benefits of postmastectomy NAC reconstruction, there is no standard, viable method for reliably reconstructing a permanent and realistic NAC. Current NAC reconstruction options are limited to tattoos, prostheses, surgical skin flap reconstructions, nipple-sharing reconstructions, and Cook Medical's BioDesign Nipple Reconstruction Cylinder.[11,20] These approaches produce NACs that are nonliving, nonpermanent, lack physical depth, or fail to maintain a projection for more than a few months or a year.[9,16,19–23] Because most surgical NAC reconstructions utilize nonhomologous soft tissue,[24] an average of 48% loss of nipple projection can occur by the end of the first-year postreconstruction.[20] In addition, current surgical approaches show variable patient satisfaction outcomes across similar reconstruction techniques—a possible result of differing expertise and skill among surgeons.[20,21,25–28] This can result in patients seeking revision surgeries when their reconstructed NACs lose projection and alter in general appearance.[20,23] NAC reconstruction is a significant unmet medical need; patients and physicians need an easy-to-apply, standardized, permanent, and aesthetically pleasing NAC reconstruction option.

To address the limitations of current NAC reconstruction approaches, we adopted a tissue engineering approach predicated upon the hypothesis that a human donor NAC could be recovered, decellularized (dcl-NAC), and serve as a nonimmunogenic scaffold for regeneration of the NAC in a recipient. We focused on deriving a biologic scaffold through decellularization rather than synthesizing scaffolds, such as hydrogels or three-dimensional printed structures, because, unlike synthesized scaffolds, native tissue matrices are highly complex, being composed of hundreds of extracellular matrix (ECM) proteins that structurally interconnect and possess unique mechanical and signaling properties.[22,29,30] In addition, we have significant experience in decellularizing numerous tissue types.[31–35]

Previously, we established a decellularization method for generating a nonhuman primate (NHP) dcl-NAC and identified the graft's ability to support cell viability and growth *in vitro*.[32] In this work, *rhesus macaque* NHP-NACs were recovered and decellularized (dcl-NHP-NACs), and then, analyzed for ECM components through proteomic and histological analyses. Dcl-NHP-NACs were further evaluated for biocompatibility and their ability to support host-mediated recellularization in *in vivo* studies in mice and a single rhesus macaque. Data from these *in vivo* studies demonstrate that dcl-NACs retain the important structural and morphological components of native NACs, including the nipple projection, and support recellularization *in vivo*. This suggests that utilizing a dcl-NAC as a scaffold for NAC regeneration, in lieu of surgical NAC reconstruction, is a feasible approach for achieving a living, permanent NAC for patients who have undergone mastectomy.

Materials and Methods

Tissue recovery and animal care

All NHP tissue samples in this study were collected from rhesus macaque (*Macaca mulatta*) adults, by Tulane National Primate Research Center (TNPRC). All donor animals were humanely euthanized under approved IACUC protocols due to chronic gastritis or as normal controls assigned to other studies. All surgical approaches were performed by a veterinarian in accordance with the NIH Guide for Care and Use of Laboratory Animals and approved by the Institutional Animal Care and Use Committee of the TNPRC (P0337). Native human skin samples were collected under an approved protocol (15-747763) for deidentified medical waste tissues by the Tulane University Biomedical Institutional Review Board. All rodent procedures conformed to the requirements of the Animal Welfare Act, and protocols (4434) were approved by the Institutional Animal Care and Use Committee at Tulane University.

Proteomic analysis of nipple

The tip of the nipple ($\sim$50 mg of tissue) was harvested from three male NHPs with an average age of 6 years old. Three native NHP-NACs and three dcl-NHP-NACs were used in proteomic analysis. Dcl-NHP-NAC were obtained by decellularizing NHP-NACs following the previously published protocol.[32] All tissue was frozen at −80°C and transferred to the Cell, Molecular, and Bioinformatics Core at Xavier University for proteomic analysis. For each tissue, the lysates were pooled ($n=3$ NHP-NACs; $n=3$ dcl-NHP-NACs) and the total protein concentration was measured with the bicinchoninic acid assay (Pierce). An equal quantity of protein was processed through trypsin digestion and desalination. Subsequent high-performance liquid chromatography with mass spectroscopy (LC-MS/MS) was performed on an LTQ-Orbitrap (Thermo Fisher) with an Ultimate 3000

Nanoflow HPLC System (Dionex) as described previously.[36] Protein data were generated using the Mascot (Matrix Science) search algorithm and Proteome Discoverer 1.2 software (Thermo Fisher Scientific).

Gene pathways related to peptide analysis

To identify the most abundant proteins in the sample, the protein dataset was sorted by peptide number, representing the quantity of peptide sequences identified from a master protein group. This provides a relative comparison of the most abundantly measured protein groups. The top 10 proteins, sorted by peptide number, were tabulated for NHP-NAC and dcl-NHP-NAC. Proteins from the native and decellularized NAC datasets were identified in the ExPASy Bioinformatics Resource Portal protein database by accession number and sorted into the following categories: cytosol/intracellular, membrane, cytoskeleton, nucleus, secreted/non-ECM, mitochondrial, ECM, and growth factors.[37] The percentage of protein in each category was calculated by dividing the total number of peptides in each by the total number of all peptides per sample. The sum of all percentages exceeds 100% because proteins were assigned to multiple categories in some cases.

All of the collected protein accession numbers were converted into a list of gene names and imported into the DAVID Bioinformatics Resource for functional gene annotation analysis.[38] The Go BP Fat database was selected and gene ontology categories were generated with a corresponding *p*-value to represent the strength of the association of the gene ontology category with the gene list.[39] The *p*-values were converted into a negative logarithmic scale and the top 10 categories were extracted with the list of genes ascribed to the functional category.

Cryoscanning electron microscopy

NHP-NAC and dcl-NHP-NAC samples were briefly fixed in 10% neutral buffered formalin then placed in phosphate-buffered saline (PBS) overnight before being transferred to water. Hydrated samples were sectioned into smaller pieces and were mounted on a cryogenic scanning electron microscopy (cryo-SEM) sample holder with a small amount of Tissue-Tek adhesive (Sakura; Ted Pella, Redding, PA). The mounted tissue was permitted to air dry for 20 min before quickly plunging into a liquid nitrogen slush and then moved into a vacuum transfer container under high vacuum. The samples were fractured in the Hitachi S-4800 Field Emission cryo-SEM chamber, to expose the inner layers of the samples. The temperature was increased to –95°C to sublime surface ice for 30 min. Next, the tissue was sputter coated with platinum and palladium in the presence of argon gas and plasma at 3.0 kV for 88 s.

Immunohistochemical analysis

Immunohistochemical (IHC) staining for endothelial cells employed a primary rabbit polyclonal antibody for platelet endothelial cell adhesion molecule (PECAM-1, CD31, catalog No. ab28364; Abcam). A horseradish peroxidase-conjugated goat anti-rabbit secondary antibody (catalog No. ab6721; Abcam) was used. The primary antibody was used at a dilution of 1:50 and the secondary antibody was used at a dilution of 1:1000. A secondary only control was used to confirm antibody specificity. After deparaffinization and rehydration with successive ethanol washes, tissue sections were boiled for 20 min in 10% sodium citrate buffer. Sections were washed twice with TBS-T solution (50 mM Tris [pH 7.6], 150 mM NaCl, 0.05% Tween-20) then blocked for 30 min with TBS-T containing 1% bovine serum albumin (catalog No. A3803; Sigma). Samples were then incubated overnight at 4°C with the primary antibody or blocking control in a humidified chamber. Samples were washed twice in TBS-T before being incubated with the secondary antibody for 1 h. After being washed with TBS-T solution, samples were processed using the ImmPACT DAB Peroxidase Substrate Kit (catalog No. SK-4105; Vector Laboratories) according to the manufacturer's protocol. Specimens were washed with PBS and then counterstained with modified Mayer's Hematoxylin (catalog No. 1202; Newcomer Solutions, Madison, WI).

Slide imaging was performed using an Olympus BX51 polarizing microscope (Olympus Scientific Solutions, Waltham, MA). At least three images per specimen were analyzed using QuPath software and ImageJ software.[40] The number of blood vessels per area was calculated and compared. Tissue embedding, sectioning, and staining were completed through the Histology Core at the Center for Stem Cell and Regenerative Medicine at Tulane University School of Medicine.

Collagen quantification

Using methods previously described, collagen I and collagen III were quantified across histological sections using Picrosirius Red.[41,42] Polarized microscopy (Olympus BX51) and MATLAB custom software were used to image and deconvolute spectral properties of Picrosirius-stained collagen within sections. Briefly, orange and red-stained fibers indicate collagen I while yellow and green-stained fibers indicate collagen III. All postimage analysis was performed across a random sampling of Picrosirius Red-stained samples within each slide. Data are represented as a ratio of collagen I:collagen III ± SEM. Tissue embedding, sectioning, and Picrosirius Red staining were completed through the Histology Core at the Center for Stem Cell Research and Regenerative Medicine at Tulane University School of Medicine.

In vivo *murine subcutaneous implants and animal care*

Mouse experiments were performed with 4-week-old C57BL/6 females. Mice were weighed, anesthetized through IP injection with ketamine and xylazine and provided analgesia administered subcutaneously with buprenorphine. Mice were shaved between the shoulder blades and back of the neck and the local area was cleaned with chlorohexidine and 70% ethanol. An incision of ~1.0 cm was made dorsally between the shoulder blades and one implant was placed subcutaneously. Implants were sized uniformly using a 1.0 cm biopsy punch. There were five groups, including controls—Surgery only (i.e., no implant), Commercial (i.e., Strattice, catalog No. 1016002; LifeCell Corporation, Branchburg, NJ), Native (i.e., N-NAC), Decell nipple group 1 (i.e., dcl-NHP-NAC), Decell nipple group 2 (i.e dcl-NHP-NAC)—with 15 mice per group.

At 2, 14, and 21 days postimplantation, five mice per group were sacrificed by CO_2 inhalation followed by

cervical dislocation, blood collected by atrial incision, and implants excised; weights were measured weekly. Two groups of dcl-NHP-NAC were included in this study to account for different batches of decellularization: Decell group 1 was decellularized ~12 months before Decell group 2; both were stored in PBS in a refrigerator until use.

Blood cells were analyzed for $CD45^+$ cells as previously described.[43,44] In brief, blood cells were labeled with $CD45^+$ (catalog No. 17-0451-82; eBioScience, San Diego, CA) antibody and flow cytometric analysis was performed using a BD LSRFortessa™ (BD Biosciences, San Jose, CA) instrument. Data analysis was acquired of 10,000 events using FlowJo software (FlowJo, LLC, Ashland, OR).

In vivo *nonhuman primate pilot study and animal care*

All surgical approaches were performed by a veterinarian in accordance with the NIH Guide for Care and Use of Laboratory Animals and a protocol approved by the Institutional Animal Care and Use Committee of the TNPRC. The chest region of an anesthetized 6-year-old, male, rhesus macaque was shaved and wiped with chlorohexidine and alcohol pads to sterilize the skin. Both nipples were removed from the host with a scalpel. The dorsal midline region was shaved and wiped with chlorohexidine and alcohol pads. Approximately 1 cm diameter round excisions of full-thickness skin were made along the dorsal midline in two columns with 10 on the left and 10 on the right. The excisions removed the epidermis, exposing the dermal bed and were evenly spaced at ~4 cm apart. The apical portion of decellularized NHP nipples were removed and onlay engrafted onto each surgically prepared dermal bed. Sutures were used to secure the grafts. The NHP's own two nipples were engrafted in the two dermal bed regions closest to the tail.

Graft sites were monitored by a veterinarian for general signs of inflammation (edema, redness) and adverse events (necrosis). Grafts with minimal surrounding host tissue were excised *en bloc* at 1-, 3-, and 6-week time points post-engraftment. Excised grafts were immediately placed into 10% neutral buffered formalin and fixed for at least 24 h at ambient temperature.

Weekly weight and peripheral blood samples, for complete blood count (CBC) and comprehensive metabolic panel (Chem12) analyses, were collected. Before any surgical event, 5 mL of peripheral blood was drawn. The CBC analysis was performed using the Sysmex XP-300 Hematology Analyzer. The Chem12 analysis was performed using a Beckman AU400 chemistry analyzer. Normal value ranges for rhesus macaque were determined empirically at TNPRC and are presented for each measured analyte in Results section.

Statistical methods

Statistical significance was determined by two-tailed *t*-tests or one-way analysis of variance with a Tukey's *post hoc* test. For all analyses, an $n=3$ or greater number of experiments were conducted. The murine study represents an $n=5$ per time point. A p-value ≤ 0.05 was considered significant and is designated by an asterisk (*); $p \leq 0.01$ is designated as **, and $p \leq 0.001$ is designated as ***. Analyses that were not found to be significant are not shown in most graphs. Numerical values are presented as average ± SEM. All calculations and graphs were completed using Prism (GraphPad software) version 8.

Results

Proteomic analysis

To better understand the proteomic similarities and differences between NHP-NAC and dcl-NHP-NAC tissues, a comprehensive, quantitative, and unbiased comparison of protein compositions was performed. Proteomic analysis of whole-tissue extracts revealed a total of 173 peptides detected in dcl-NHP-NACs as compared with 456 peptides in NHP-NACs. The total detected proteins were binned according to their subcellular localization (Fig. 1A). In NHP-NACs, most proteins were identified as cytosolic (27.82%) and secreted/non-ECM (25.59%), which was similar to dcl-NHP-NACs (20.14% cytosolic; 22.66% secreted/non-ECM). Of note, dcl-NHP-NACs were greatly enriched for ECM proteins (12.59%) as compared with NHP-NACs (3.54%). Membrane-associated proteins were similar (NHP-NACs, 14.17%; dcl-NHP-NACs, 14.39%); cytoskeletal proteins were greater in dcl-NHP-NACs (15.11%) than NHP-NACs (8.79%); and nuclear proteins and mitochondrial proteins were higher in NHP-NACs.

The 10 most abundant proteins identified in both native and decellularized groups are listed (Fig. 1B). NHP-NACs show an abundance of cytosolic structural proteins, such as filamin-A, vimentin, and prelamin-A/C, whereas dcl-NHP-NACs shows primarily collagen IV and I. Of note, blood proteins were heavily present in the NHP-NAC, making up 5 out of the 10 most abundant proteins identified, including: transferrin derivatives, serum albumin, and alpha-2-macroglobulin derivatives.

When the proteomic data were correlated with DAVID, a cell signaling pathway online database, functional gene pathways were cross-referenced and a gene ontology was generated (Fig. 2). NHP-NACs had proteins in cell signaling pathways most highly associated with glycolysis, metabolic processes, and catabolic processes, whereas, the dcl-NHP-NACs' proteins were most highly associated with epidermal and ectodermal differentiation. The metabolic processes associated with the NHP-NAC proteins are representative of enzymatic processes performed by soluble intracellular proteins, whereas those associated with dcl-NHP-NAC proteins are insoluble proteins related to tissue structure and cell migration.

Next, for the dcl-NHP-NACs, the top 10 proteins from each of the cell signaling pathways identified (Fig. 2) were then crossreferenced with each other to illustrate overlap of protein function and to identify key proteins that play multiple cellular functions (Fig. 3). It was found that collagen I, collagen III, collagen VI, and laminin played roles in multiple pathways, with more than four pathways per protein. All processes identified from the dcl-NHP-NACs are adhesion-dependent processes, as was expected. The dcl-NHP-NACs tissue should be largely devoid of soluble proteins that are associated with signaling and cellular activity. Since the cells have been removed, we found primarily the insoluble networks of proteins that play roles in structure and migration guidance.

Decellularized nipple structure

Using this decellularization approach, it was found that dcl-NHP-NACs retain their gross morphology as evidenced by maintenance of a nipple projection, cylindrical nipple shape, and a visually well-maintained tissue volume (Fig. 4A). The

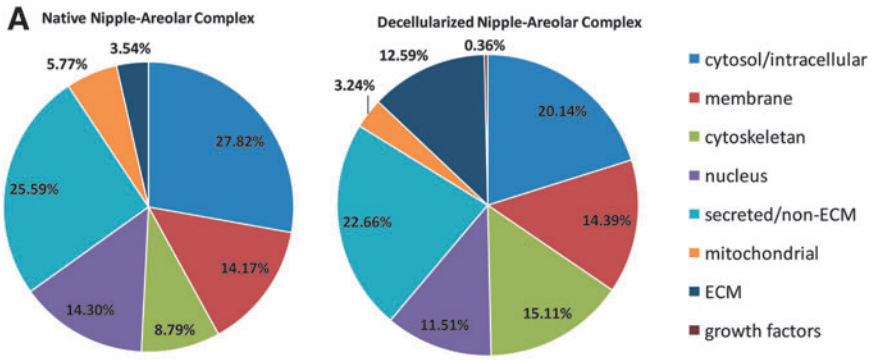

B

Rank	Description	No. of Peptides
Native Nipple-Areolar Complex		
1	Filamin-A isoform 1	63
2	Serum albumin	44
3	C3 and PZP-like alpha-2-macroglobulin domain-containing protein 1	37
4	Transferrin	31
5	Transferrin	30
6	Alpha-2-macroglobulin	27
7	Vimentin	24
8	Prelamin-A/C isoform 1	22
9	Vinculin isoform	22
9	Talin-1	19
Decellularized Nipple-Areolar Complex		
1	*Collagen alpha-3(VI) chain isoform 4*	46
2	*Collagen alpha-3(VI) chain*	44
3	*Fibrillin-1*	29
4	Myosin-11 isoform SM1A	25
4	Myosin-11	25
6	*Collagen alpha-1(I) chain preproprotein*	22
7	Serum albumin	21
8	*Collagen alpha-1(VI) chain*	20
9	*Collagen alpha-2(VI) chain, isoform 2C2A*	20
9	*Cytokeratin-1*	19

FIG. 1. Protein localization of native and decellularized rhesus-derived nipple tissue. **(A)** Graphs from analysis of proteomic data showing the percentage of all detected proteins as sorted by subcellular localization. Percentages are based on the total count of detected peptides. **(B)** The 10 most abundant proteins identified in both native and decellularized groups. ECM, extracellular matrix.

most notable difference is the absence of pigmentation, which, under native conditions, is primarily due to melanin within the epidermis and the underlying microvasculature. Using a previously described approach,[41,42] collagen I and collagen III content was measured across histological sections to determine if dcl-NHP-NACs retained similar quantities of this crucial scaffold protein compared with NHP-NACs (Fig. 4B) and no difference was found. These data suggest that the insoluble collagen I and III within NAC tissue is largely unchanged postdecellularization.

NHP-NACs and dcl-NHP-NACs were evaluated qualitatively using cryo-SEM. This approach provides super-resolution topological imaging of samples in their largely native and nondistorted form. The epidermis of native tissue, as compared with decellularized, appeared coarser with more furrows and ridges, however, the furrows were larger within the decellularized tissue (Fig. 4C, D). Higher magnification images of the underlying dermis were imaged. Large bundled structures were observed in both samples and presumed to be collagen (Fig. 4E, F). The bundled nature of this collagen was

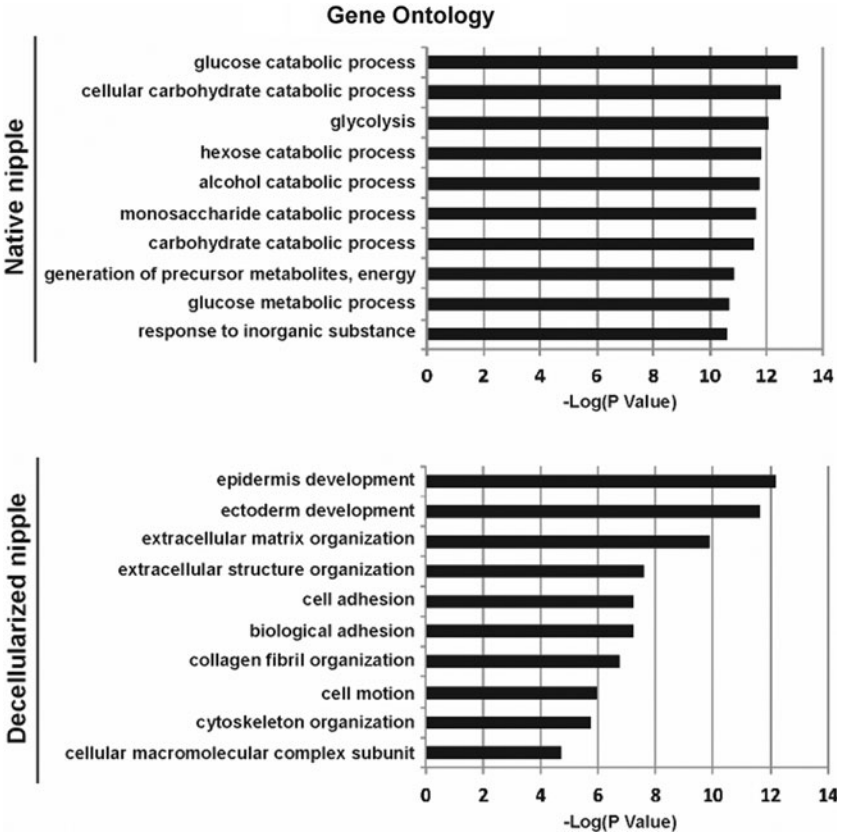

FIG. 2. Gene ontology of the top 10 gene pathways related to peptide analysis. Proteins to Functional Gene Pathway Relationship shows the functional analysis of the proteomics data using the relationship of all identified proteins to functional gene ontology groups as identified by the DAVID Bioinformatics Resource.

more compact in native tissue than decellularized. Closer magnification of bundled structures revealed fibers. These appeared slightly more condensed in the native versus decellularized tissue samples (Fig. 4G, H). Interestingly, fiber orientation and alignment with neighboring fibers appeared similar between samples. Taken together, similar physical structures and relative quantity of structures were identified between native and decellularized tissue samples; however, decellularized nipple tissue appeared less dense than native tissue, likely due to the removal of cellular content.

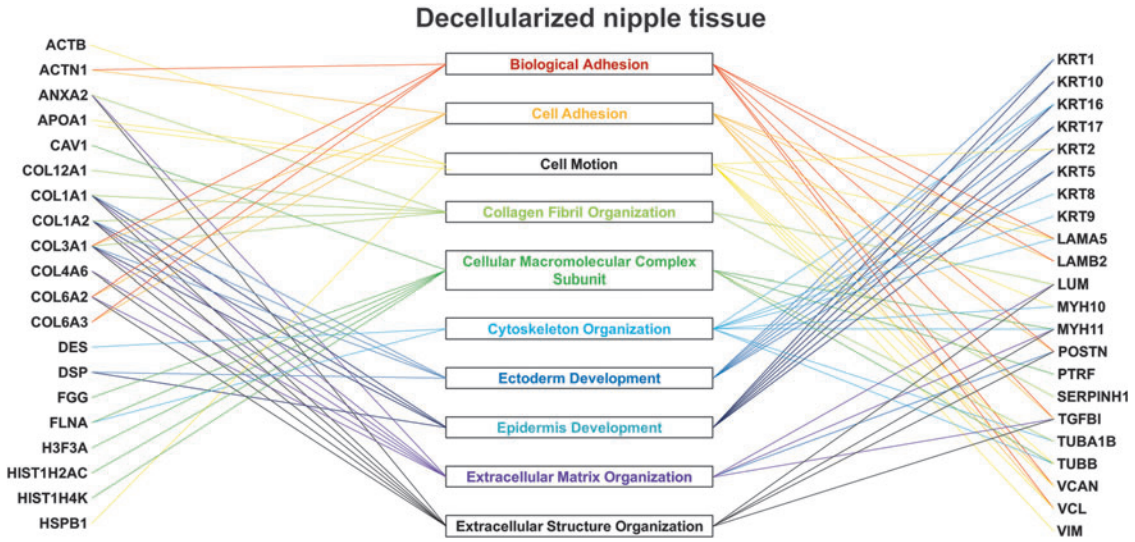

FIG. 3. Mapping key proteins to functional gene pathways. From the top 10 most highly correlated gene pathways of dcl-NHP-NACs, the genes were mapped to show the crossover between protein and gene pathways, illustrating the important roles and multiple pathways of collagen I, collagen III, and collagen VI, as well as keratins and laminins. NAC, nipple–areolar complex; NHP, nonhuman primate.

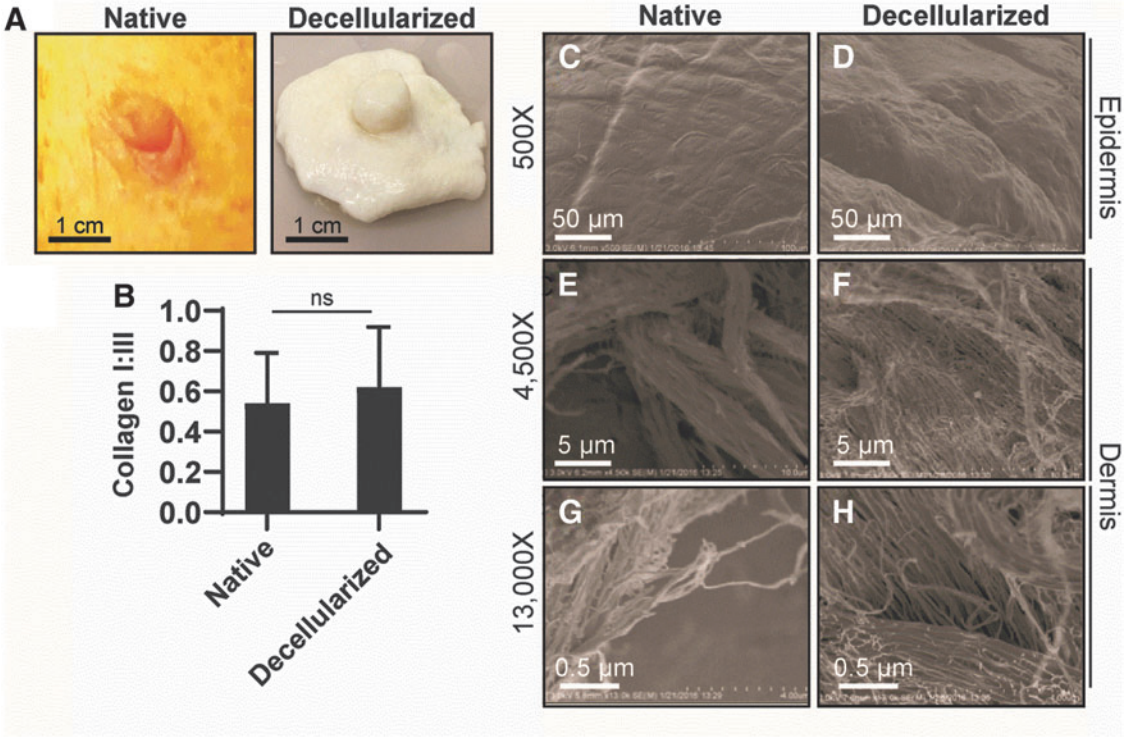

FIG. 4. Structure of the rhesus macaque nipple. **(A)** Photographs of an NHP-NAC (native) and dcl-NHP-NAC (decellularized). **(B)** Graph of collagen I:III levels in native and decellularized NACs. Student's *t*-test. ns, nonsignificant ($p > 0.05$). **(C–H)** Scanning electron cryomicroscopy images of native and decellularized NACs. **(C, D)** Micrographs showing the epidermis. **(E–H)** Micrographs showing the dermis at different magnification.

In vivo *murine subcutaneous implants and biocompatibility*

In an effort to understand the biocompatibility and bioactivity of dcl-NHP-NACs, grafts were implanted subcutaneously in mice as described in the methods section. At 2, 14, and 21 days postimplantation, five mice per group were sacrificed, blood collected, and implants excised; weights were measured weekly. Changes in body weight and $CD45^+$ (common leukocyte antigen) levels provide insight into the host systemic inflammatory response to implanted tissues. Over the course of this study, we found no differences in weight among the Surgery Only group, Native control group, Decell nipple group 1, and Decell nipple group 2 (Fig. 5M, analysis not shown). However, the Commercial group showed significant differences in weight on day 2 and 21 as compared with Surgery only and Native control groups.

Analysis of blood samples for $CD45^+$ cells showed similar levels for Surgery only group, Decell nipple group 1, and Decell nipple group 2 for all time points (Fig. 5N). $CD45^+$ cell levels were lower in the Native control group than Surgery only group, Decell nipple group 1, and Decell nipple group 2 on day 14; however, this trend was opposite on day 21.

The bioactivity of implants was measured based on levels of neovascularization. Neovascularization was determined by counting grouped cells across slides that stained positive for $CD31^+$ (PECAM-1) and showed open lumens (Fig. 5F–J). Analysis of neovascularization showed no difference among Commercial group, Decell nipple group 1, and Decell nipple group 2 at day 14, but an increase in neovascularization was measured at day 21 in Decell nipple group 2 (Fig. 5O). Importantly, for all groups, an increase in neovascularization was observed over time. Decell nipple groups 1 and 2 showed the greatest mean values for $CD31^+$ cells/field. Decell nipple group 2 showed an increase in $CD31^+$ cells/field over Commercial group.

Analysis of histological sections from Decell nipple groups 1 and 2 showed the presence of cells within the tissue stroma as well as red blood cell (RBC)-containing blood vessels, suggesting functioning *de novo* vasculature (Fig. 5A–E, K, L). Interestingly, the sutures in three mice failed, thus exposing the decellularized nipple implant to the air; reepithelialization was observed over the implants (Fig. 5K, L), demonstrating that the decellularized nipple implants support ingrowth from surrounding tissue as well as epithelial recellularization, *in vivo*.

In vivo *NHP pilot study*

The dcl-NHP-NACs were assessed for biocompatibility and recellularization in a single, adult male rhesus macaque. The rhesus macaque is widely used in a variety of preclinical applications and is ideal for studying humoral responses and regenerative functions in a nearest-to-human animal model. Briefly, 18 dcl-NHP-NACs and two native host nipples were onlay engrafted on partial-thickness wound beds prepared along the dorsal midline (Fig. 6A). The dcl-NHP-NACs were nipple portions encompassing ~ 1 cm of the top portion of the nipple. Each circular nipple graft was ~ 1 cm in diameter. All grafts were sutured onto the wound bed and

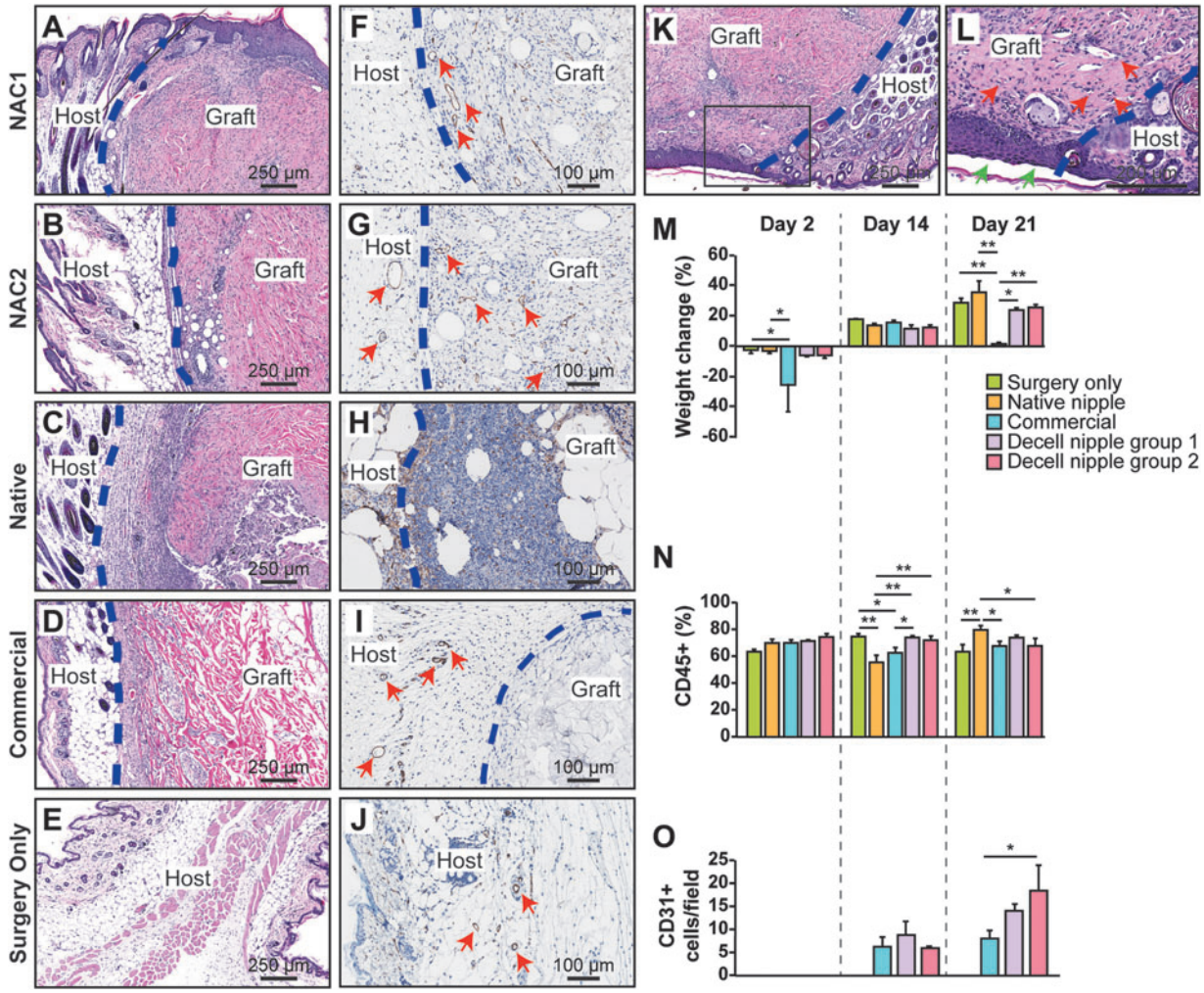

FIG. 5. Subcutaneous implant mouse study. **(A–E)** H&E stains of decellularized nipple implants from 21 days post-implantation. **(F–J)** $CD31^+$ stains of implants 21 days postimplantation. **(K)** Decellularized nipple implant exposed to air showing reepithelialization of implant. **(L)** Magnified *black box* region in **(K)**. *Green arrows* point to epithelium. *Red arrows* point to blood vessels. **(M)** Graph showing percent weight change relative to day 0 weight of mice. **(N)** Graph of percent $CD45^+$ (common leukocyte antigen). **(O)** Graph of $CD31^+$ cells per field that were detected from histological analyses of resected grafts over time. One-way ANOVA with Tukey's *post hoc* test was performed. $*p < 0.05$; $**p < 0.01$. ANOVA, analysis of variance.

bandaged. Gross animal weight was measured and blood samples collected for complete blood cell counts and analysis of metabolite levels from periods before (8 months), during (6 weeks), and after (2.5 months) the study.

During the 8-month period before surgery, the average weight was 19.50 ± 0.57 lbs. There was a significant increase in weight ~1-month before the engraftment portion of the study that persisted for 1 week (Fig. 6B). This weight gain was transient and soon decreased to 19.51 lbs 10 days before surgery, where it remained steady at 18.92 ± 0.20 lbs during the 6-week period of the study. A slight decrease in weight occurred following the graft resection at weeks 1, 3, and 6, reflecting a 4.9%, 4%, and 6% decrease, respectively. This pattern likely reflects the repeated graft excisions. After complete removal of all grafts, weight was on average 19.19 ± 0.44 lbs. No significant changes were detected in average weights from before, during, and after the study.

NHP study blood cell counts

Total erythrocyte counts (RBC) showed a gradual increase over the course of the study (Fig. 6C). A significant increase in erythrocyte counts was found between the periods before and after the study; however, no significant differences were found between the periods before or after the study and the study period. All counts measured were within the normal range ($4.10–7.80 \times 10^6$ cells/μL). A consistent trend was not observed with regard to cell count changes and graft harvest time points. After engraftment (week 0), a slight decrease in counts was observed; however, an increase in counts was observed after graft resections at week 1 (see week 2). These counts decreased after graft resections at week 3 (see week 4).

Erythrocyte properties were measured for hemoglobin (Hgb), hematocrit (Hct), and cell size (Supplementary Fig. S1). Hgb reflects the iron-containing oxygen-transport

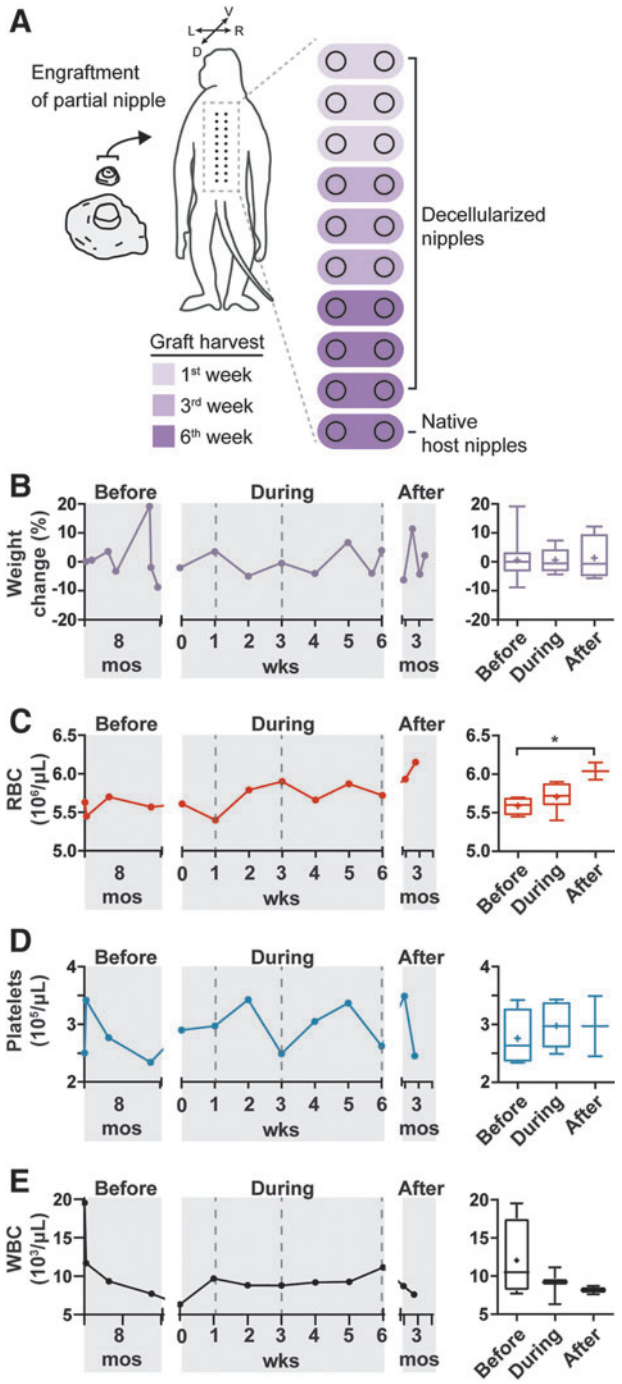

FIG. 6. NHP pilot study. **(A)** Illustration showing animal study design. The apical portion of decellularized rhesus macaque NACs was used for onlay engraftment along the dorsal midline of an adult rhesus macaque. The top 9 rows were decellularized partial nipples (18 total) while the *lower row* (closest to tail) was the primate's own nipples (2 total). Grafts were harvested at 1, 3, and 6 weeks postengraftment. **(B)** Graph of animal weight. **(C)** Graph of RBC counts. **(D)** Graph of platelet counts. **(E)** Graph of WBC counts. *Dashed lines* in each graph represent graft harvest time points. Graphs of averaged values from periods of study are shown to the right for body weight, RBCs, platelets, and WBCs. One-way ANOVA with Tukey's *post hoc* test was performed. $*p < 0.05$. ANOVA, analysis of variance; RBC, red blood cell; WBC, white blood cell.

ability of erythrocytes. Hgb values were within the normal range and remained stable during the study; no changes were detected among periods before, during, and after the study. Hct reflects the number of erythrocytes in blood. An increase in Hct was detected between the periods before and after the study, which is consistent with the trend observed in the RBC counts. No difference between the periods before and after the study was observed for the mean corpuscular volume (Mcv), which reflects the physical volume of erythrocytes. A decrease in the value of mean corpuscular hemoglobin (Mch) was detected between periods before and after the study. The Mch measures the mass of Hgb per cell. No differences were observed for the Mch concentration, which measures the average concentration of Hgb per cell. Lastly, the RBC distribution width (Rdw) measures the variance across the range of RBC sizes with a high value reflecting a broad distribution of sizes and a lower value reflecting a small distribution of sizes. No difference in Rdw was observed between periods before and after the study. All values were within the normal ranges for each.

Platelet counts were within the normal range during the entire study ($1.93–6.76 \times 10^5$ cells/μL) (Fig. 6D). The 8-month period before the study showed large fluctuations in platelet counts and may reflect an acute infection/illness. Increases in platelet counts were observed following weeks 1, 3, and 6 graft resections; however, this response was transient with levels decreasing within 1–2 weeks after resections. Despite the overall trend showing frequent changes over time, no significant changes were measured before, during, and after the study.

Total white blood cell (WBC) counts remained steady, without significant deviations, over the entire study with no detectable changes occurring before, during, or after the study (Fig. 6E). All cell count values were within the normal range and did not show obvious trends over time. Approximately 8 months before the start of the study, counts were out of the normal range ($6.6–15.5 \times 10^3$ cells/μL) with a value of 19.54×10^3 cells/μL; however, counts returned within normal range 6 days later (11.68×10^3 cells/μL). All values for neutrophils (Neu), lymphocytes (Lym), monocytes (Mon), eosinophils (Eos), and basophils (Bas) were within normal range and no differences were observed among periods before, during, and after the study (Supplementary Fig. S2). These data suggest that the dcl-NHP-NACs do not elicit an adverse systemic immune response.

NHP study graft recellularization

Harvested grafts were histologically analyzed for recellularization, focusing on neovascularization and reepithelialization (Fig. 7). For neovascularization, the lumen area of microvasculature within the grafts were measured over time. Slides of dcl-NHP-NACs, resected at weeks 1, 3, and 6, and control NHP-NACs, resected at week 6, were stained with H&E (Fig. 7E, F) to validate microvasculature. A clear increase in lumen area was observed over the study with a significant increase between weeks 1 and 3, but no significant difference between weeks 3 and 6 (Fig. 7H); these data provide evidence in support of active neovascularization that reached a steady state at 3 weeks postengraftment. Furthermore, there was no significant difference in vessel lumen area between test and control grafts resected at week 6,

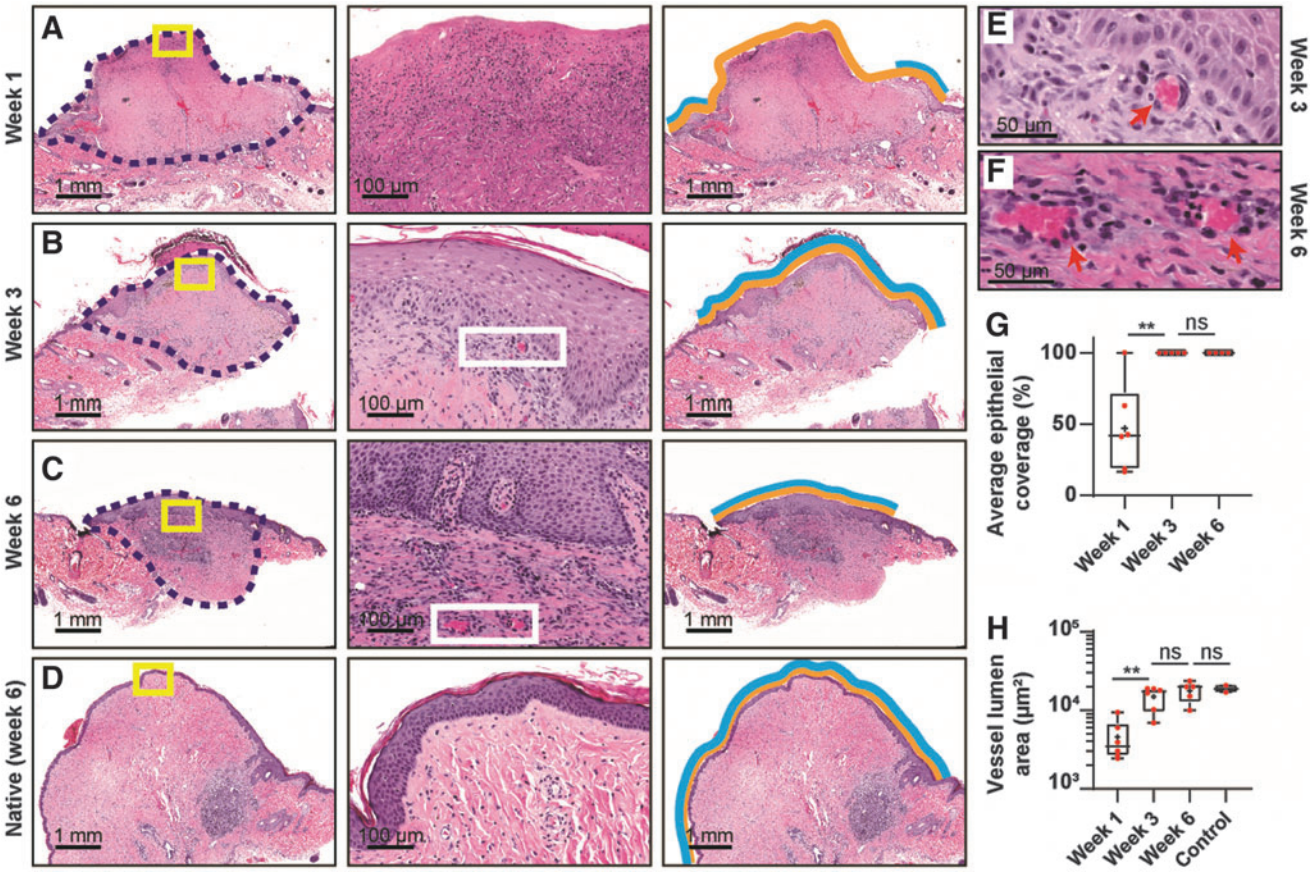

FIG. 7. NHP-mediated recellularization of decellularized nipple grafts. Examples of NHP-nipple grafts resected after **(A)** 1 week postengraftment, **(B)** 3 weeks postengraftment, and **(C)** 6 weeks postengraftment. **(D)** The native NHP-nipple after 6 weeks postengraftment. The *second column* shows magnified regions of the *yellow boxes* in the *first column* of **(A–D)**; and the *third column* indicates how epithelialization coverage was calculated: *yellow lines* are the entire exposed area of the grafts and *blue lines* are the reepithelialized region of the exposed grafts. **(E, F)** Magnified regions from *white boxes* in **(B, C)** showing examples of neovascularization (*red arrows*). **(G)** Graph of average epithelial coverage of nipple grafts over time. **(H)** Graph of blood vessel lumen area from nipple grafts over time. The control sample is of the host's native nipples from 6 weeks postengraftment. One-way ANOVA with Tukey's *post hoc* test was performed in **(G, H)**. $^{**}p < 0.01$. ns, not significant.

suggesting that dcl-NHP-NACs have revascularized to a level similar to that found in NHP-NACs within 6 weeks.

For reepithelialization, the distance new epidermis migrated from the edge (as indicated by blue lines in third column of Fig. 7) of the dcl-NHP-NACs as compared with the total edge-to-edge distance of the grafts (as indicated by yellow lines in third column of Fig. 7) was measured. By week 3, dcl-NHP-NACs showed complete reepithelialization (Fig. 7G), which remained unchanged through the end of the study.

Discussion

The protein composition of the dcl-NAC is important as it defines the chemical and mechanical properties of the scaffold, which are critical for providing proper spatial cues to infiltrating cells; ECM protein composition and architecture are associated with changes in the ability of cells to repopulate a scaffold.[45] These proteomic analyses demonstrate relative enrichment of the percentage of structural ECM proteins in the dcl-NHP-NACs. For example, the dcl-NHP-NACs showed enrichment for collagen (I, III, and VI), fibrillin, and laminin matrix proteins and for cytoskeletal proteins, including actin, desmin, filamin, keratin, myosin, and vimentin. Interestingly, all of these proteins are relatively insoluble, suggesting that the decellularization procedure removes primarily soluble cytosolic and nuclear proteins. It is unclear whether the presence of cytoskeletal proteins facilitate or hinder the recellularization of a dcl-NAC, but the structural function of these proteins may contribute to its mechanical integrity. The presence of collagen, fibrillin, and laminin matrix proteins is promising for the ability of a dcl-NAC to recapitulate the mechanical properties and microarchitecture of a native NAC.

The retention of collagen-alpha-I and collagen-III in the dcl-NHP-NACs is consistent with the Picrosirius Red staining. Prior work from our group showed through IHC staining that laminin is preserved,[32] which is consistent with the proteomics dataset. Although fibrillin is prominent in the dcl-NHP-NACs' proteomics dataset, elastin is notably absent from both the NHP-NACs and dcl-NHP-NACs. We previously showed that elastin content was significantly

reduced after decellularization, however, it was detectable through oxalic acid extraction.[32] The inconsistency between our previously published IHC data and the current proteomics data for elastin may reflect loss of this protein in the insoluble pellet that is not measured by LC-MS/MS for proteomics analysis. Transforming growth factor-β, the secreted growth factor detected in dcl-NHP-NACs, serves an important role in ECM remodeling, angiogenesis, and epithelialization, which may be of functional value for recellularization.

Gene ontology analysis identified the genetic pathways with the greatest representation in the protein datasets, incorporating both the number of genes associated with the pathways and the degree to which those genes are integral to the pathways. The strongest gene ontology association with NHP-NACs involved multiple cellular metabolic pathways, whereas dcl-NHP-NACs had strong associations with ECM structure/organization and epidermis/ectoderm development. These features of the protein environment in dcl-NHP-NACs are encouraging and support the regenerative potential of a dcl-NAC and its ability to maintain sufficient structural integrity necessary to mimic native NACs. Additional gene ontology categories with strong representation in dcl-NHP-NACs included functions of cell/biological adhesion and cell migration, which may facilitate reepithelialization.[46–48]

Analysis of the proteome by LC-MS/MS of detergent-mediated decellularized tissue is limited because this process may differentially affect the native and decellularized tissue, regarding ECM proteins in particular.[49] Some proteins are poorly solubilized and are discarded before detection; for example, the insoluble pellet from decellularized lung has been shown to be rich in fibrillar ECM proteins.[49] Nonetheless, the LC-MS/MS of dcl-NHP-NACs in this study demonstrates the enrichment of ECM proteins. In fact, collagen-alpha-1, which is notably absent from the protein datasets of decellularized tissue in the literature,[49] was detected as the sixth most abundantly measured peptide in the dcl-NHP-NAC here. It is possible that the dcl-NHP-NACs contain even more ECM proteins than detected by the proteomics analysis in this study. Of note, a relative comparison of the abundance of peptide by LC-MS/MS measurements is presented in this study, but the comparison does not provide absolute quantitative information about protein levels in the tissue samples. Quantitative methods of proteomics analysis may provide more detailed information about the protein composition of the scaffold in future studies.

It is known that collagen I and collagen III work in concert to play an essential role in ECM strength and elasticity.[50] By comparing the proportion of collagen I to collagen III from native to decellularized samples, it can be hypothesized that the mechanical properties are maintained after the decellularization of the NACs, and that the decellularization process does not significantly affect the mechanical properties through the loss or alteration of the ratio of collagen I to collagen III. Follow-up studies will be conducted to evaluate the mechanical properties of human-derived NAC grafts.

In the *in vivo* murine model, no significant differences were observed in changes in weight or $CD45^+$ among Surgery Only, Decell nipple group 1, and Decell nipple group 2 throughout the study. Through CD31 IHC analysis, neovascularization of the dcl-NHP-NACs was observed at a similar level to or statistically greater than the Commercial group at days 14 and 21. In addition, the sutures for three mice failed, likely due to the animal rubbing against the cage, thus exposing the dcl-NHP-NACs to air; and interestingly, through H&E staining, a new epidermal layer was visible. These observations suggest that dcl-NACs are biocompatible and support recellularization.

The *in vivo* NHP pilot study was designed to evaluate the biocompatibility of dcl-NHP-NACs on a rhesus macaque. It also provided a proof of concept for the surgical engraftment of dcl-NACs onto a human-like host, demonstrating both safety and tolerability with the engraftment procedure. The gross body weight, CBC, and Chem12 data (data not shown) collected from before, during, and after the study show that the dcl-NHP-NACs do not elicit an adverse systemic reaction and are biocompatible. This result likely speaks to the inert nature of the allogeneic grafts after our decellularization process and to the onlay engraftment approach. Furthermore, the dcl-NHP-NACs were found to be well integrated with the host and capable of progressing through normal healing, within the 6-week study.

The slight decrease in body weight that was observed after resection of grafts from weeks 1, 3, and 6 may reflect appetite suppression as a result of anesthesia and surgery. Despite these slight changes, overall weight did not differ among periods of the study. These data suggest that the engraftment procedure and dcl-NHP-NACs themselves do not elicit adverse effects on gross body weight.

Similar to transient changes observed in body weight after graft resections, platelet counts were found to increase at these same time points. The increased platelet counts after resection likely reflects increased clotting from repeated bleeding events. Platelet levels appeared to have decreased to steady state, suggesting a return to normalcy, after all grafts were removed. Despite these transient changes, average platelet counts did not differ among periods of the study, confirming they were reflective of acute events.

Erythrocyte counts seemed to follow an increasing trend over the life of the study with an increase occurring after week 1, a decrease after week 3, and an increase after week 6. The significant increase in average erythrocyte count between periods before and after the study may reflect increased erythrocyte production in response to repeated bleedings. Another cause of increased erythrocyte count is dehydration, although none of the electrolyte results supports this with salt levels (Na^+, K^+, Cl^-) remaining unchanged (data not shown). Erythrocyte properties showed slight changes between periods before and after the study. For example, Hct levels showed an increase between periods before and after the study, whereas Mch showed a decrease in Hgb per cell for the same periods. The decrease in Mch was expected to be mirrored in the Mcv since a larger cell tends to contain more Hgb; however, a significant decrease in Mcv was not detected. Furthermore, no difference in Rdw was detected, suggesting sizes of erythrocytes remained relatively constant. Increased erythrocyte counts were mirrored with an apparent increase in Hgb and a statistical increase in Hct, as expected. The decrease in Mch along with the increase in erythrocyte count may reflect systemic changes in hemostasis caused by frequent bleedings during graft resections.

Leukocyte counts were steady over the entire study and did not show any significant changes among periods before,

during, and after the study. Despite the engraftment and resection of multiple grafts within a relatively short period, the systemic inflammatory response was relatively constant, suggesting the animal did not experience an adverse inflammatory response and did not reject the grafts. The histology data do show some regions of high local WBC infiltrates within the grafts at week 1 with a gradual decrease in the occurrence toward 6 weeks postengraftment. Elucidating the identity and timeframe for resolution of these inflammatory processes would provide insight into whether they are acute or chronic; however, such evaluation was beyond the scope of the current study.

Our data show that we are able to adequately decellularize a complex, dense tissue such as the NAC, removing all detectable intact cells and any immunogenic properties, and that dcl-NACs are biocompatible and support recellularization without rejection of the grafts by the hosts. Given these findings, the decellularization process for generating the dcl-NHP-NACs in this study will be used for deriving human dcl-NACs in future studies. Our preliminary efforts in manufacturing human dcl-NACs from deceased donor NACs support the use of a similar decellularization process for human NAC tissue. Although only the nipple of the dcl-NHP-NACs was used in this study, future studies will be performed using human dcl-NACs that contain the entire nipple and, depending on the study design (referring to size limitations of the host), some amount of the areola.

Conclusions

Our studies of the dcl-NHP-NACs show significant data that the decellularization process allows us to generate a dcl-NAC that is biocompatible and supports recellularization. Our proteomic and cryo-SEM data showed that dcl-NACs are enriched in structural ECM and cytoskeletal proteins and that the microarchitecture is sufficiently intact. Our *in vivo* murine study showed that dcl-NACs are biocompatible and support neovascularization and, anecdotally, reepithelialization. Furthermore, the *in vivo* NHP feasibility study served as a proof of concept for surgical engraftment of dcl-NACs, which will inform future animal and clinical studies using human dcl-NACs. Data from gross weight and CBC values that were collected over the entire study showed no evidence in support of any adverse systemic responses. The histology data clearly showed good host-mediated recellularization of the dcl-NACs. The rate of recellularization was relatively rapid with complete reepithelialization and obvious neovascularization evident 6 weeks after engraftment. In summary, these data suggest that a dcl-NAC is a viable solution for regeneration of the NAC for patients who have suffered a breast cancer-related mastectomy.

A limitation of this study was that only the nipples, not the nipple and the surrounding areola region, were used in the proteomic analysis and the *in vivo* NHP feasibility study. It is expected that the nipple and areola are made up of a similar proteomic profile, with the exception of different ratios of collagen I:III. The intended use in clinic would be to engraft human-derived dcl-NAC grafts, including the surrounding areola, onto a deepithelialized dermal bed of a reconstructed breast. It is expected that these larger grafts would also reepithelialize and revascularize, as observed in this study, with cells migrating in from the surrounding host tissues. Future studies will build off of the data presented in this study and will assess the biocompatibility and host-mediated recellularization of larger human-derived dcl-NACs.

Acknowledgments

The authors thank Dina Gaupp, Cyndi Trygg, Maury Duplantis, Allison Rosenberg, PhD, and Jibao He, PhD for their help with the logistics, specimen collection and preparation, and support for this project.

Author Contributions

N.C.P., B.A.B., S.S., B.J.B., A.C.B., R.A.S., D.M.G., W.M.H., K.S.M., and A.E.C. helped in initial experimental design and/or writing/editing of article. N.C.P., V.C.C., W.M.H., J.H., E.C.M., B.O. R.A.S., B.J.B., and B.G. carried out experimentation.

Disclosure Statement

N.C.P., W.M.H., D.M.G. and V.C.C. were all employed during the preparation of this article and own stock in the company. B.A.B. and S.S. are scientific advisors to the company. All other authors declare no competing interest.

Funding Information

N.C.P. and B.O. were supported by an NSF IGERT Fellow training grant in Bioinnovation, DGE-1144646. The Tulane National Primate Research Center; NIH grant number OD 11104. BioAesthetics Corporation provided funding for the NHP pilot study and publication expenses.

Supplementary Material

Supplementary Figure S1
Supplementary Figure S2

References

1. NIH SEER Program. Cancer Stat Facts: Female Breast Cancer. National Cancer Insitute, 2019. From: https://seer.cancer.gov/statfacts/html/breast.html. Accessed November 12, 2019.
2. American Cancer Society. Breast Cancer Facts & Figures 2017–2018. Atlanta, GA: American Cancer Society, Inc., 2017.
3. Howlader, N., Noone, A.M., and Krapcho, M. SEER Cancer Statistics Review, 1975–2014, based on November 2016 SEER data submission, posted to the SEER web site, April 2017. Bethesda, MD: National Cancer Institute, 2017. Lung Cancer Screening, Version. 2017:3.
4. Steiner, C.A., Weiss, A.J., Barrett, M.L., Fingar, K.R., and Davis, P.H. Trends in Bilateral and Unilateral Mastectomies in Hospital Inpatient and Ambulatory Settings, 2005–2013. HCUP Statistical Brief #201. Rockville, MD: Agency for Healthcare Research and Quality, 2016.
5. Azouz, S., Swanson, M., Omarkhil, M., and Rebecca, A. A nipple-areola stencil for three-dimensional tattooing: nipple by number. Plast Reconstr Surg **145,** 38, 2020.
6. Romanoff, A., Zabor, E.C., Stempel, M., Sacchini, V., Pusic, A., and Morrow, M. A Comparison of patient-reported outcomes after nipple-sparing mastectomy and conventional mastectomy with reconstruction. Ann Surg Oncol **25,** 2909, 2018.

7. Goh, S.C.J., Martin, N.A., Pandya, A.N., and Cutress, R.I. Patient satisfaction following nipple-areolar complex reconstruction and tattooing. J Plast Reconstr Aesthet Surg **64,** 360, 2011.
8. Ghosh, S., Shaw, A., and Watson, J. Nipple reconstructions: comparison of patients' and surgeons' perspectives. Breast **6,** 42, 1997.
9. Chia, H.-L., Wong, M., and Tan, B.-K. Nipple reconstruction with rolled dermal graft support. Arch Plast Surg **41,** 158, 2014.
10. Davis, G.B., Miller, T., and Lee, G. Nipple reconstruction: risk factors and complications. In: Shiffman, M.A., ed. Nipple-Areolar Complex Reconstruction: Principles and Clinical Techniques. Cham, Switzerland: Springer International Publishing, 2018, pp. 619–627.
11. Riesel, J.N., and Chun, Y.S. Reconstruction of the nipple-areola complex. In: Shiffman, M.A., ed. Nipple-Areolar Complex Reconstruction: principles and Clinical Techniques. Cham, Switzerland: Springer International Publishing, 2018, pp. 351–358.
12. Ibrahim, A.M.S., Lau, F.H., Sinno, H.H., Lee, B.T., and Lin, S.J. Analyzing patient preference for nipple-areola complex reconstruction using utility outcome studies. In: Shiffman, M.A., ed. Nipple-Areolar Complex Reconstruction: Principles and Clinical Techniques. Cham, Switzerland: Springer International Publishing, 2018, pp. 661–668.
13. Bykowski, M.R., Emelife, P.I., Emelife, N.N., Chen, W., Panetta, N.J., and de la Cruz, C. Nipple-areola complex reconstruction improves psychosocial and sexual well-being in women treated for breast cancer. J Plast Reconstr Aesthet Surg **70,** 209, 2017.
14. Spector, D.J., Mayer, D.K., Knafl, K., and Pusic, A. Women's recovery experiences after breast cancer reconstruction surgery. J Psychosoc Oncol **29,** 664, 2011.
15. Jabor, M.A., Shayani, P., Collins, D.R., Karas, T., and Cohen, B.E. Nipple-areola reconstruction: satisfaction and clinical determinants. Plast Reconstr Surg **110,** 457, 2002.
16. Momoh, A.O., Colakoglu, S., De Blacam, C., *et al.* The impact of nipple reconstruction on patient satisfaction in breast reconstruction. Ann Plast Surg **69,** 389, 2012.
17. Didier, F., Arnaboldi, P., Gandini, S., *et al.* Why do women accept to undergo a nipple sparing mastectomy or to reconstruct the nipple areola complex when nipple sparing mastectomy is not possible? Breast Cancer Res Treat **132,** 1177, 2012.
18. Delay, E., Mojallal, A., Vasseur, C., and Delaporte, T. Immediate nipple reconstruction during immediate autologous latissimus breast reconstruction. Plast Reconstr Surg **118,** 1303, 2006.
19. Collins, B., Williams, J.Z., Karu, H., Hodde, J.P., Martin, V.A., and Gurtner, G.C. Nipple reconstruction with the biodesign nipple reconstruction cylinder: a prospective clinical study. Plast Reconstr Surg Global Open **4,** e832, 2016.
20. Kristoffersen, C.M., Seland, H., and Hansson, E. A systematic review of risks and benefits with nipple-areola-reconstruction. J Plast Surg Hand Surg **51,** 287, 2017.
21. Jalini, L., Lund, J., and Kurup, V. Nipple reconstruction using the C-V flap technique: long-term outcomes and patient satisfaction. World J Plast Surg **6,** 68, 2017.
22. Khoo, D., Ung, O., Blomberger, D., and Hutmacher, D.W. Nipple reconstruction: a regenerative medicine approach using 3D-printed tissue scaffolds. Tissue Eng Part B Rev **25,** 126, 2019.
23. Shestak, K.C., Gabriel, A., Landecker, A., Peters, S., Shestak, A., and Kim, J. Assessment of long-term nipple projection: a comparison of three techniques. Plast Reconstr Surg **110,** 780, 2002.
24. Yanaga, H., and Yanaga, K. Nipple-Areola complex reconstruction with dermal-fat flaps: technical improvement from rolled auricular cartilage to artificial bone. In: Shiffman, M.A., ed. Nipple-Areolar Complex Reconstruction: Principles and Clinical Techniques. Cham, Switzerland: Springer International Publishing, 2018, pp. 393–402.
25. Satteson, E.S., Brown, B.J., and Nahabedian, M.Y. Nipple-areolar complex reconstruction and patient satisfaction: a systematic review and meta-analysis. Gland Surg **6,** 04, 2017.
26. Mohamed, S.A., and Parodi, P.C. A modified technique for nipple-areola complex reconstruction. Indian J Plast Surg **44,** 76, 2011.
27. Germanò, D., De Biasio, F., Piedimonte, A., and Parodi, P.C. Nipple reconstruction using the fleur-de-lis flap technique. Aesthetic Plast Surg **30,** 399, 2006.
28. Henderson, J.T., Lee, T.J., Swiergosz, A.M., Hiller, A.R., Choo, J., and Wilhelmi, B.J. Nipple-Areolar complex reconstruction: a review of the literature and introduction of the rectangle-to-cube nipple flap. Eplasty **18,** e15, 2018.
29. Kular, J.K., Basu, S., and Sharma, R.I. The extracellular matrix: structure, composition, age-related differences, tools for analysis and applications for tissue engineering. J Tissue Eng **5,** 2041731414557112, 2014.
30. Vogel, V. Unraveling the mechanobiology of extracellular matrix. Annu Rev Physiol **80,** 353, 2018.
31. Bonvillain, R.W., Scarritt, M.E., Pashos, N.C., *et al.* Non-human primate lung decellularization and recellularization using a specialized large-organ bioreactor. J Vis Exp e50825-e, 2013.
32. Pashos, N.C., Scarritt, M.E., Eagle, Z.R., Gimble, J.M., Chaffin, A.E., and Bunnell, B.A. Characterization of an acellular scaffold for a tissue engineering approach to the nipple-areolar complex reconstruction. Cells Tissues Organs **203,** 183, 2017.
33. Thomas-Porch, C., Li, J., Zanata, F., *et al.* Comparative proteomic analyses of human adipose extracellular matrices decellularized using alternative procedures. J Biomed Mater Res A **106,** 2481, 2018.
34. Matossian, M.D., Burks, H.E., Bowles, A.C., *et al.* A novel patient-derived xenograft model for claudin-low triple-negative breast cancer. Breast Cancer Res Treat **169,** 381, 2018.
35. Scarritt, M.E., Pashos, N.C., Motherwell, J.M., *et al.* Re-endothelialization of rat lung scaffolds through passive, gravity-driven seeding of segment-specific pulmonary endothelial cells. J Tissue Eng Regen Med **12,** e786, 2018.
36. Scarritt, M.E., Bonvillain, R.W., Burkett, B.J., *et al.* Hypertensive rat lungs retain hallmarks of vascular disease upon decellularization but support the growth of mesenchymal stem cells. Tissue Eng Part A **20,** 1426, 2014.
37. Artimo, P., Jonnalagedda, M., Arnold, K., *et al.* ExPASy: SIB bioinformatics resource portal. Nucleic Acids Res **40,** W597, 2012.
38. Huang, D.W., Sherman, B.T., and Lempicki, R.A. Systematic and integrative analysis of large gene lists using DAVID bioinformatics resources. Nat Protoc **4,** 44, 2009.
39. Huang, D.W., Sherman, B.T., and Lempicki, R.A. Bioinformatics enrichment tools: paths toward the com-

prehensive functional analysis of large gene lists. Nucleic Acids Res **37,** 1, 2009.
40. Bankhead, P., Loughrey, M.B., Fernández, J.A., *et al.* QuPath: open source software for digital pathology image analysis. Sci Rep **7,** 16878, 2017.
41. Bersi, M.R., Collins, M.J., Wilson, E., and Humphrey, J.D. Disparate changes in the mechanical properties of murine carotid arteries and aorta in response to chronic infusion of angiotensin-II. Int J Adv Eng Sci Appl Math **4,** 228, 2013.
42. Udelsman, B.V., Khosravi, R., Miller, K.S., *et al.* Characterization of evolving biomechanical properties of tissue engineered vascular grafts in the arterial circulation. J Biomech **47,** 2070, 2014.
43. Bowles, A.C., Strong, A.L., Wise, R.M., *et al.* Adipose stromal vascular fraction-mediated improvements at late-stage disease in a murine model of multiple sclerosis. Stem Cells **35,** 532, 2017.
44. Bowles, A.C., Wise, R.M., Gerstein, B.Y., *et al.* Immunomodulatory effects of adipose stromal vascular fraction cells promote alternative activation macrophages to repair tissue damage. Stem Cells **35,** 2198, 2017.
45. Welham, N.V., Chang, Z., Smith, L.M., and Frey, B.L. Proteomic analysis of a decellularized human vocal fold mucosa scaffold using 2D electrophoresis and high-resolution mass spectrometry. Biomaterials **34,** 669, 2013.
46. Gál, P., Vasilenko, T., Kostelníková, M., *et al.* Open wound healing in vivo: monitoring binding and presence of adhesion/growth- regulatory galectins in rat skin during the course of complete re-epithelialization. Acta Histochem Cytochem **44,** 191, 2011.
47. Livigni, A., Peradziryi, H., Sharov, A.A., *et al.* A conserved Oct4/POUV-dependent network links adhesion and migration to progenitor maintenance. Curr Biol **23,** 2233, 2013.
48. Gallant-Behm, C.L., Du, P., Lin, S.M., Marucha, P.T., DiPietro, L.A., and Mustoe, T.A. Epithelial regulation of mesenchymal tissue behavior. J Invest Dermatol **131,** 892, 2011.
49. Hill, R.C., Calle, E.A., Dzieciatkowska, M., Niklason, L.E., and Hansen, K.C. Quantification of extracellular matrix proteins from a rat lung scaffold to provide a molecular readout for tissue engineering. Mol Cell Proteomics **14,** 961, 2015.
50. Gelse, K., Pöschl, E., and Aigner, T. Collagens—structure, function, and biosynthesis. Adv Drug Deliv Rev **55,** 1531, 2003.

Address correspondence to:
Bruce A. Bunnell, PhD
Department of Pharmacology
Tulane University School of Medicine
1430 Tulane Avenue, SL-99
New Orleans, LA 70112
USA

E-mail: bbunnell@tulane.edu

Received: August 16, 2019
Accepted: January 7, 2020
Online Publication Date: March 2, 2020